Biophysics and Physicobiology

Regular Article

Dynamic and static analyses of glass-like properties of three-dimensional tissues

Hironobu Nogucci

Graduate School of Arts and Sciences, The University of Tokyo, Meguro-ku, Tokyo 150-8902, Japan

The mechanical properties of tissues are influenced by those of constituent cells in various ways. For instance, it has been theoretically demonstrated that two-dimensional confluent tissues comprising mechanically uniform cells can undergo density-independent rigidity transitions, and analysis of the dynamical behavior of tissues near the critical point revealed that the transitions are geometrically controlled by the so-called cell shape parameter. To investigate whether three-dimensional tissues behave similarly to two-dimensional ones, we herein extend the previously developed model to three dimensions both dynamically and statically, demonstrating that two mechanical states similar to those of glassy materials exist in the three-dimensional case. Scaling analysis is applied to the static model focused from the rearrangement viewpoint. The obtained results suggest that the upper critical dimension of tissues equals two and is therefore the same as that of the jamming transition.

Key words: tissues and organs, epithelial–mesenchymal transition, jamming transition, glass

Cell rearrangement is frequently observed in confluent tissues and plays important roles during developmental processes, wound healing, and cancer metastasis [1]. The above processes have many common features and are therefore categorized as epithelial–mesenchymal transitions (EMTs). Notably, epithelial cells are tightly packed, i.e., located in close proximity to each other, while the packing of mesenchymal cells is more loose. During EMT, the mechanical properties of a tissue change from those of the epithelial state to those of the mesenchymal state, while the opposite phenomenon is denoted as MET. These macroscopic states reflect individual cell mechanical properties such as cortical tension and intercellular adhesion that are regulated by gene expression.

From the viewpoint of physics, EMT can be described as being analogous to two well-known phase transitions. For instance, the mechanical rigidity of epithelial tissues and the fluid-like nature of mesenchymal tissues suggest that their interconversion can be modeled by a solid-to-liquid phase transition. However, epithelial cells feature an irregular configuration and behave similarly to glassy materials, most of which undergo a jamming transition upon packing rate (ρ) change. However, confluent tissues experience EMT even when the packing rate is kept constant ($\rho=1$) [2]. Alternatively, EMT can be modeled by phase transitions induced by the collective motions of active matter components [3,4]. In particular, active matter comprises particles that move indi-

Corresponding author: Graduate School of Arts and Sciences, The University of Tokyo, 3-8-1 Komaba, Meguro-ku, Tokyo 153-8902, Japan.
e-mail: noguchi@complex.c.u-tokyo.ac.jp

◀ *Significance* ▶

Changes in the mechanical properties of individual cells comprising three-dimensional tissues are shown to induce a transition affording a glass-like state. In view of the fact that the above properties (e.g., elasticity, contractility, and surface tension) are strongly dependent on single cell shape, tissue stiffness can be estimated by imaging of constituent cells. Moreover, since a similar relationship between cell shape and tissue stiffness has previously been reported for a two-dimensional case, the upper critical dimension of tissues may equal two, which is the same as that of the material jamming transition.

vidually by consuming energy supplied from outside, with notable multi-scale examples being flocks of birds, groups of cells, and intracellular components, and the cooperative motion of these particles results in the formation of dynamic collective orders. However, active matter phase transitions are accompanied by density changes, which is not the case for EMT.

EMT has been extensively experimentally studied, particularly in two-dimensional systems. For instance, a Bayesian force inference was proposed to measure the distribution of forces on the edges between two contacting cells in developmental processes [5], and the above method was employed to show that mechanical anisotropy promotes cell packing with hexagonal ordering in *Drosophila* pupal wing [6]. Additionally, structural reconstructions of laser ablation–produced holes in epithelial sheets were investigated in the context of wound healing [7], while breast cancer cells were demonstrated to undergo individual pulsating migrations in epithelial tissues due to mechanical property mismatch, which provided insights into tumor progression [8,9]. Moreover, tracking of individual cells and their glassy behavior such as caging and dynamic heterogeneity was employed to analyze collective cell motions within tissues [10].

Recently, Bi *et al.* observed a new type of phase transition in two-dimensional tissues comprising mechanically uniform cells [11,12], employing a model with a phenomenological energy functional (E) originating from cellular shape. In particular, E can be viewed as the sum of individual cell energies E_i, which in turn, can be expressed as

$$E_i = K_A(A_i - A_0)^2 + \xi P_i^2 + \gamma P_i \tag{1}$$

where A_i, P_i, K_A, ξ, γ, and A_0 are the mean area and perimeter of cell i, the cell's elastic constant in two-dimensional systems, active contractility driven by cytoskeletons present in cells, interfacial tension between contacting cells, and the optimal area of an isolated cell, respectively, while $\widetilde{P} = -\gamma/2\xi$, introduced as a "shape parameter," is the optimal cell perimeter in the energy ground state. The energy cost of cell rearrangement vanishes at $\widetilde{P} > \widetilde{P}_0$, and the rigidity transition was found to occur at $\widetilde{P}_0 \approx 3.81$, at which value the optimal cell shape corresponds to a regular pentagon. Furthermore, collective cell motions drastically change at $\widetilde{P} \approx \widetilde{P}_0$. While individual cells move diffusively if $\widetilde{P}$ and the magnitude of self-propelling velocity v_0 are large, some are caged by their surrounding cells, and the collective motion is heterogeneous elsewhere.

Despite the abovementioned insights, the behavior of three-dimensional tissues has not been investigated to date, and the existence of a rigidity transition in three-dimensional cases remains to be elucidated. Herein, we extend the energy functional E to a three-dimensional system and model individual cell energy E_i as

$$E_i = K_v(V_i - V_0)^2 + K_A(A_i - A_0)^2, \tag{2}$$

where V_i and V_0 represent cell volume and its optimal value in a single-cell system, respectively, while K_v represents the cell's elastic constant in three-dimensional systems [13].

In this study, collective cell behavior in three-dimensional confluent tissues was investigated using dynamical and static models. The settings used to model dynamical cell motions are explained, and the corresponding results demonstrate that the phase transition of collective motions is similar to a glass transition and is influenced by a shape parameter introduced later in the text. To investigate static behavior around the transition, cell rearrangement energy was measured and analyzed by a scaling method described. Finally, conclusions and discussion are presented.

Methods

Model equations

The Voronoi cell model used in a previous work [12] was employed to describe collective cellular motion considering cell shape. In this model, the position and orientation of cell i are represented as x_i ($= (x_i, y_i, z_i)$) and p_i ($= (p_{xi}, p_{yi}, p_{zi})$), respectively. Specifically, cell position is denoted by the cell center, and cell orientation is denoted by a unit vector pointing from the cell tail to the cell head. Cell shape is approximated through a graphic representation generated by a three-dimensional Voronoi tessellation of $\{x_i\}$ (although neighboring cells may not be in contact with each other), and gaps between cells are filled with a viscous fluid. The above approximation implies that (i) cell shape must be represented by a convex polyhedron and (ii) there should be no vacant space in the system. Throughout this paper, the boundary condition is set to be periodic, and Euler's polyhedron formula leads to the following relation: $\#f - \#e + \#v = 2$, where $\#f$, $\#e$, and $\#v$ denote the total number of faces, edges, and vertices of a single cell, respectively. A vertex connects three edges if degeneracy is ignored, which results in the relation $\#2e = 3\#v$. These relations reveal that $\#e$ and $\#v$ can be directly derived if $\#f$ is known.

We assume that (i) forces acting on cell i are described as $F_i = -\nabla_i E$ and have the same form as that described previously [12] and (ii) the magnitude of cellular self-propulsion is constant and equals v_0. In this model, neighboring cells are not necessarily in contact with each other, while their shapes are approximated by assuming cell-to-cell contacts. The action–reaction principle is balanced between a floating cell and the surrounding fluid; however, the fluid force is ignored. Based on the overdamped equation of motion, cell position x_i can be expressed as

$$\dot{x}_i = \mu F_i + v_0 p_i. \tag{3}$$

Cell orientation is assumed to be randomly perturbed within the plane perpendicular to the orientation:

$$\dot{p}_i = \nu \eta_i(t) \times p_i, \tag{4}$$

Table 1 Shape parameter ($\widetilde{A}_0$) values of regular polyhedra.

shape	$\widetilde{A}_0$
sphere	4.836
icosahedron	5.148
dodecahedron	5.312
truncated octahedron	5.315
octahedron	5.719
cube	6

where μ is the mass of each cell divided by the drag coefficient, and v denotes the moment of inertia divided by the rotational drag coefficient. The random vector $\eta_i(t) = (\eta_{i_x}(t), \eta_{i_y}(t), \eta_{i_z}(t))$ obeys the following statistics:

$$\langle \eta_{i_k}(t)\eta_{i_k}(t)\rangle = 2D\delta_{ij}\delta_{kk'}\delta(t - t'), \tag{5}$$

where δ_{ij} and $\delta_{kk'}$ are the Kronecker delta on cell indices and the component indices of the vector, respectively, while $\delta(t - t')$ is the Dirac delta function of time variables, and D is the magnitude of the orientational change of cell motion. The developed model of collective cellular motion was denoted as the self-propelled Voronoi (SPV) model.

Rescaling and parameter settings

E_i can be expressed as

$$E_i = K_V V_0^2(\widetilde{V}_i - 1)^2 + K_A V_0^{4/3}(\widetilde{A}_i - \widetilde{A}_0)^2, \tag{6}$$

where $\widetilde{V}_i = V_i/V_0$ and $\widetilde{A}_i = A_i/V_0^{2/3}$ are the rescaled volume and surface area, respectively. $\widetilde{A}_0$ depends on cell mechanical properties and denotes the optimal surface area per unit volume that minimizes the shape energy functional if the shape of all cells is confined to be equal, convex, and isotropic (Table 1). In this paper, this parameter is referred to as the "shape parameter."

For simplification, we select the unit length of the system as $V_0^{1/3}$ and set $V_0 = 1$. The system size L is set to $L = 6V_0^{1/3}$, and the total number of cells N is set to $N = 6^3$ so that the packing ratio NV_0/L^3 equals unity. The energy ratio, defined as $\gamma = K_A/(K_V V_0^{1/3})$, is fixed at $\gamma = 1$.

Some parameters determining cell properties are also fixed, i.e., $\mu = 1$, $v = 1$, and $D = 0.1$. The cell position is randomly partitioned for initial configuration.

Numerical simulations are performed until $t = 22000$ (time unit = $1/(\mu K_V V_0)$) at a fixed step size of $\Delta t = 0.1$. The statistical values of all parameter regions are calculated by averaging the results obtained for five different samples under different initial conditions.

From the geometrical viewpoint, $\widetilde{A}_0$ is related to the Kelvin problem, which poses the question of how space can be partitioned into cells of equal volume with the least surface area. If all cells are assumed to have identical shapes, the least surface area is observed for a truncated octahedron [14].

Results and Discussion

Dynamical cell behavior

Diffusive and sub-diffusive collective motion

Two distinct types of collective motion are observed on changing the parameter values v_0 and $\widetilde{A}_0$. If both v_0 and $\widetilde{A}_0$ are small, cell rearrangement is hardly observed, and collective motion is as slow as that in glass, while fast and fluid-like collective motion is observed when v_0 and $\widetilde{A}_0$ are large.

To quantitatively characterize these motions, we measured the mean squared displacement (MSD) of cell trajectories (Fig. 1). $MSD(t)$ is defined as $MSD(t - t') = \sum_{i=1}^{N}|x_i(t) - x_i(t')|^2N, t' = 2000$, where $|\cdot|$ is the L–2 norm with the periodic boundary. For all parameter regions, $MSD(t)$ is proportional to t^2 when t is small, i.e., ballistic motion is dominant at this time scale. At large t, $MSD(t)$ is proportional to t if both v_0 and $\widetilde{A}_0$ are large. However, $MSD(t)$ is proportional to t^d ($d<1$) when either diffusive or sub-diffusive motions are observed for a long period depending on parameter values.

To investigate the origin of time scale–dependent $MSD(t)$ behavior, we first divide the two time scales by the length scale of $MSD(t)$. For cell rearrangement, cells must move as far as $\sim 0.01V_0^{1.3}$, which is comparable to the edge length of a single cell. Self-propulsion is dominant before cells move further away, as shape force or diffusion is dominant after cell rearrangement.

Second, we characterize long-term collective motions and introduce $D_0 = v_0^2/3D$ as a unit of self-diffusivity, with the magnitude of self-diffusivity D_s measured as $D_s = \lim_{t\to\infty}MSD(t)/6t$. Practically, D_s can be measured by averaging $MSD(t)/6t$ for a value of t that satisfies $MSD(t) > 0.01$. If D_s/D_0 is larger than the noise floor–derived threshold, the collective motion is regarded as diffusive; otherwise, it is considered to be sub-diffusive. The threshold value is set to 0.05. Figure 2 shows the phase diagram of collective motions obtained as a result of setting the threshold. Around the threshold, the value of D_s/D_0 sharply increases with increasing $\widetilde{A}_0$.

Long-term diffusive collective motions are observed when the magnitude of self-propulsion (v_0) and the shape parameter ($\widetilde{A}_0$) are large, whereas sub-diffusive motions are observed if both of these parameters are small. The critical point $\widetilde{A}_{0*}$ in the limit $v_0 \to 0$ exceeds 5.4, although the critical point for the regular packing of a truncated octahedra equals 5.31. This point is of particular interest because cell dynamics above this value is purely dominated by the force originating from the shape energy functional, except for the noise effect, and cells can freely rearrange. The exact critical point and behavior near this point are discussed later in the manuscript.

Similarities with glassy materials

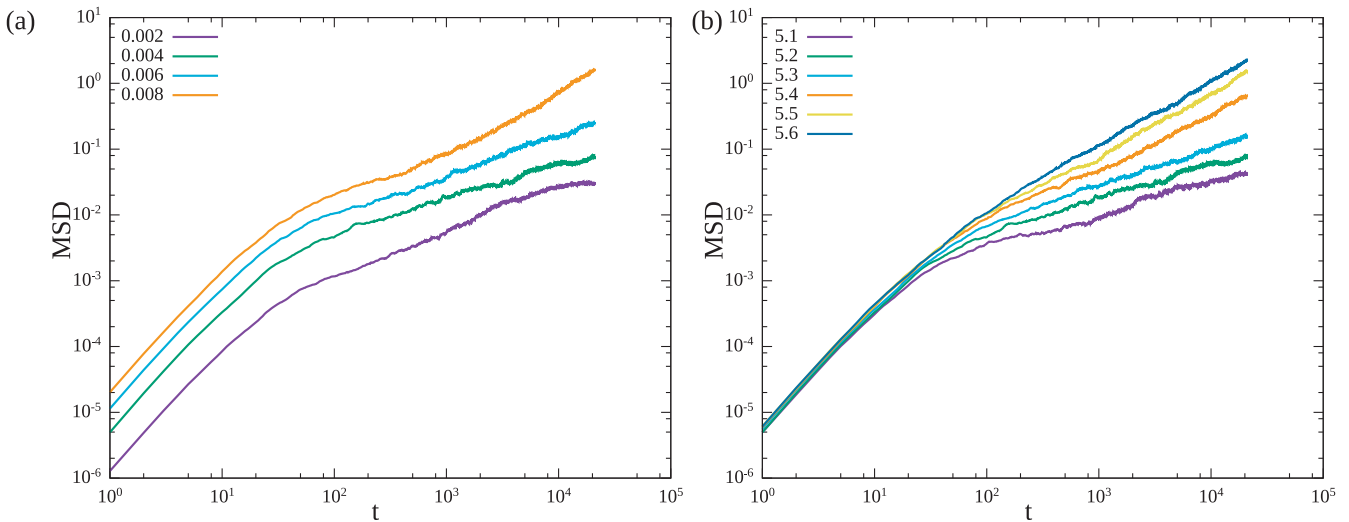Next, we consider the properties of sub-diffusive motions ($d<1$) and address the question of how these motions are

(a)

(b)

Figure 1   Time-dependent MSDs of cell trajectories determined for (a) variable v_0 and fixed $\widetilde{A}_0$ (=5.1) and (b) variable $\widetilde{A}_0$ and fixed v_0 (=0.004).
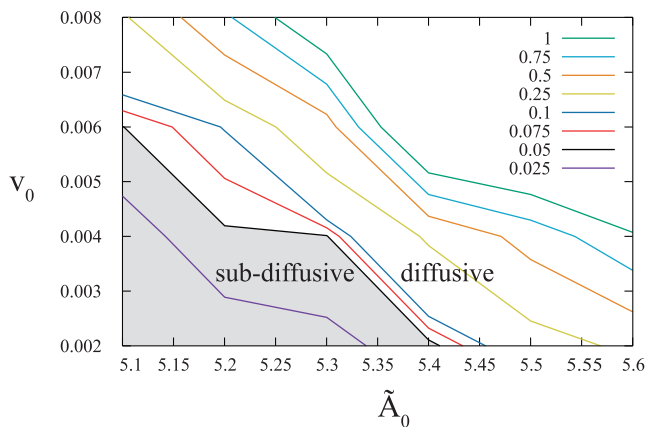

Figure 2   Contour graph of D_s/D_0 as a function of v_0 and $\widetilde{A}_0$. The black line represents the D_s/D_0=0.05 threshold. Sub-diffusive collective motions are observed in the gray-colored region, whereas diffusive motions are observed otherwise.

Figure 3   Self-intermediate scattering function ($F_s(k,t)$, $k=\pi/r_0$, t_0=2000) for different $\widetilde{A}_0$ and fixed v_0 (=0.004).

similar to that of glassy materials.

The first common example could be "caging," a phenomenon that is observed when particles cannot move as they are surrounded by their nearest neighbors for a long period of time [2] and represented by the self-intermediate scattering function $F_s(k,t)$. The above function is defined as $F_s(k,t)=\langle e^{ik\cdot\Delta r(t)}\rangle$, where $\Delta r(t)$ denotes the difference between cell positions at the start time t_0 and the measured time (t_0=2000) while $\langle\cdot\rangle$ represents the average over all cells. Figure 3 shows the values of $F_s(k,t)$ after averaging the angles of k for different parameters. The magnitude of k is fixed so that $F_s(k,0)\equiv1$, ($k=\pi/r_0$), where r_0 is the averaged nearest distance of contacting cells for each cell. If caging occurs, the value of $F_s(k,t)$ is maintained near unity for a long period of time. For a fixed value of v_0=0.004, $\widetilde{A}_0$<5.3, $F_s(k,t)$ still has a high value at the end-time of numerical
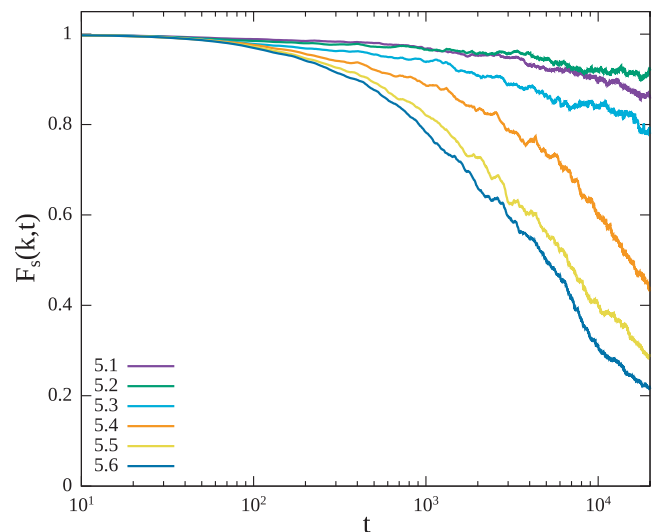
simulations. Elsewhere, the function approaches zero with increasing time, and the coefficients of curves have almost the same order ($\sim exp(10^{-4}t)$), which indicates that the tissue structure is completely relaxed within the end-time of numerical simulations.

The second common example corresponds to dynamic heterogeneity [2]. Figure 4 depicts cell migration vectors, which are defined as vectors pointing from the starting position to the finish position determined on a 10^3 time scale (t=21000–22000). In the parameter region that allows diffusive collective motions but is near the sub-diffusive region boundary, some cells move for a long distance, while others stay in small domains for a long time. This indicates that dynamical heterogeneity is also detected near the diffusive–
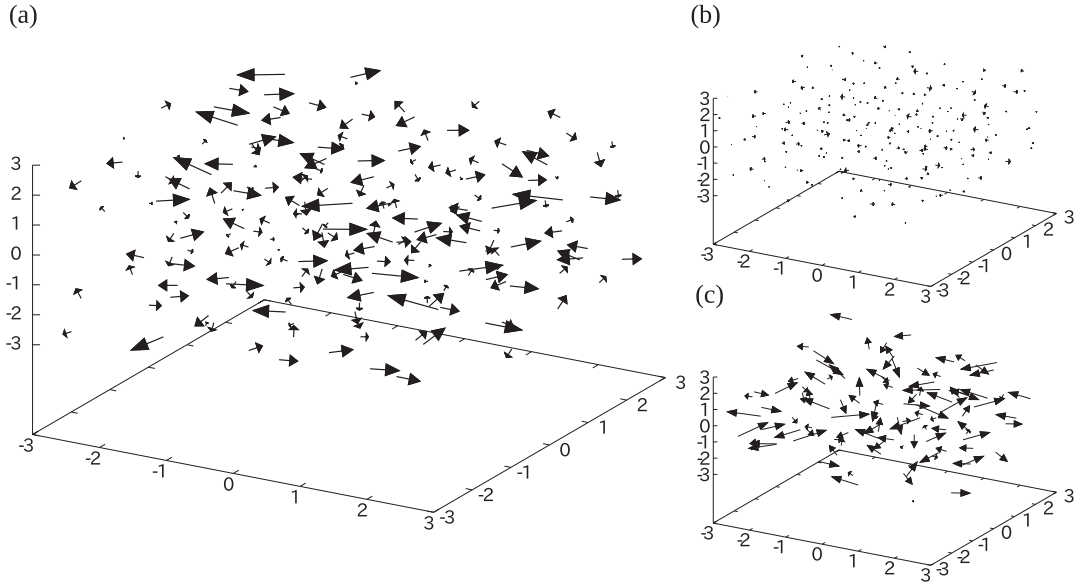
(a)

(b)

(c)

Figure 4 Migration vectors of cells determined for three different parameter sets. Duration is set as t=21000–22000. Snapshots in (a) are obtained using a diffusive parameter set near the transition boundary line ($\widetilde{A}_0$=5.4, v_0=0.004), while those in (b) are obtained using a sub-diffusive parameter set far from the boundary line ($\widetilde{A}_0$=5.1, v_0=0.002), and those in (c) are obtained using a diffusive parameter set far from the boundary line ($\widetilde{A}_0$=5.6, v_0=0.008).

sub-diffusive transition boundary line and suggests that the dynamics of three-dimensional tissues is similar to that of glass.

Analysis of individual cell shape

To understand the relationship between individual cell shape and collective motions, we measured the distributions of cell shapes. In the adopted model system, cell shape is approximated by convex polyhedra. Figure 5 shows the effect of $\widetilde{A}_0$ on the number of cell faces at fixed v_0 (=0.004), revealing that in the parameter region where collective motion is sub-diffusive, the average number of faces equals 14. At higher $\widetilde{A}_0$, when diffusive collective motion is observed, the average number of faces exceeds 15 and features a variance larger than that observed for $\widetilde{A}_0$<5.3.

Common phenomena have been observed for two-dimensional tissues, in which case an increase of the shape index triggered the "sub-diffusive"-to-"diffusive" transition [12].

The lattices of regular truncated octahedrons are the global solutions for the Kelvin proble These polyhedra have 14 faces and therefore probably represent the average shape of individual cells in the sub-diffusive collective motion regime. In two-dimensional tissues, however, the critical point corresponds to a shape parameter value representing a regular pentagon, although the global solution for the energy minimum states is represented by a regular hexagon. Therefore, we investigated actual cell shapes in three-dimensional tissues to determine whether these shapes typically correspond to regular truncated octahedra. These polyhedra feature six regular squares and eight regular hexagons as faces,
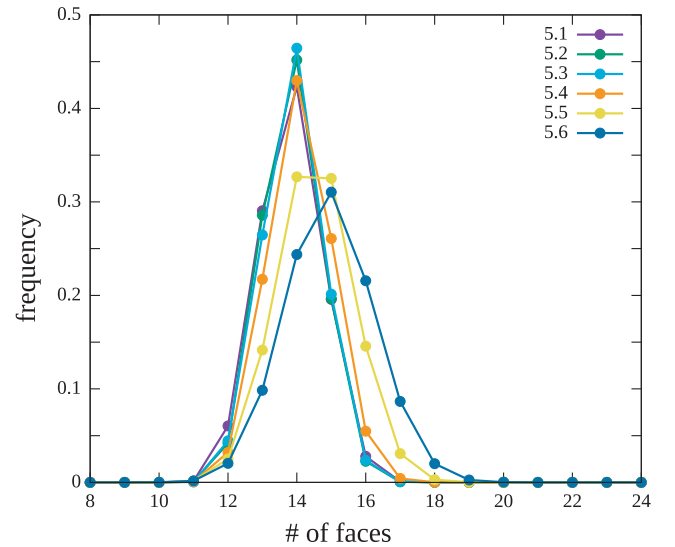
Figure 5 Distributions of polyhedra for different parameters $\widetilde{A}_0$ at constant v_0=0.004 averaged for t=21000–22000.

and the areas corresponding to unit volume equal 0.1984 and 0.5155 for square and hexagonal faces, respectively. Figure 6 shows the joint distribution for faces that belong to an n-faced polyhedron and have a specific area value. The distribution for the 14-faced polyhedron showing sub-diffusive motion features a single peak with a value of ~0.4 as the area value (Fig. 6(a)), which indicates that cell shapes are not similar to regular truncated tetrahedra. Although the lattice of a regular truncated polyhedron is the global solution of the Kelvin problem, such polyhedra does not have an iso-
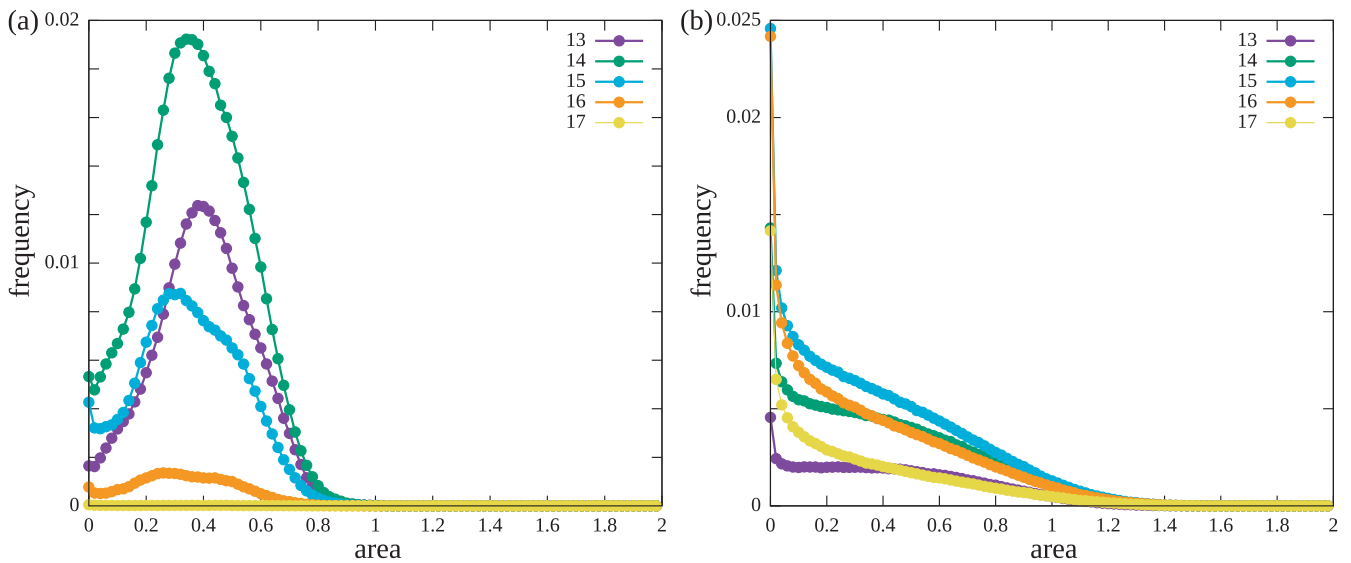
Figure 6 Joint distributions of faces belonging to an *n*-faced polyhedoron with a different area value obtained for (a) a sub-diffusive parameter set ($\widetilde{A}_0$=5.1, v_0=0.004) and (b) a diffusive parameter set ($\widetilde{A}_0$=5.6, v_0=0.008).
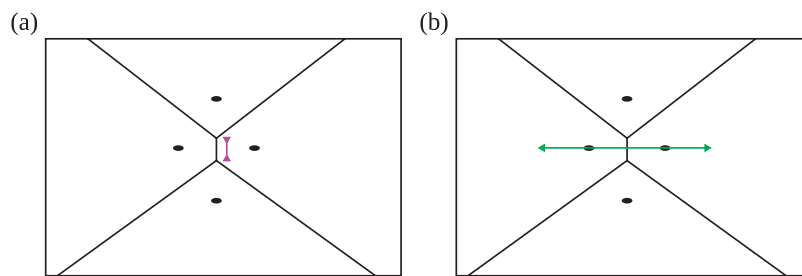

Figure 7 Schematic representations of (a) the measurement method of the CVM model in [1] and (b) the measurement method of the SPV model used in the present work. Only a two-dimensional scenario is considered for simplicity.

tropic shape. Both model equations and the periodic boundary cube do not have the mechanism to break the symmetry of isotropy for a single cell.

Moreover, the area 0 peak is always found for all faces in case of diffusive motion (Fig. 6(b)), i.e., cell rearrangement occurs for any cell shape. Diffusive collective motions originate from free cell rearrangements.

Critical point and scaling behavior of cell rearrangement energy

In the previous section, we investigated the transition from sub-diffusive collective motions to diffusive collective motions on a large time scale; however, the value of the critical point $\widetilde{A}_{0*}$ in the limit $v^0 \rightarrow 0$ remains unknown. Therefore, we aimed to determine the above value and study critical behavior in the proximity of this value by ignoring self-propulsion. To determine the value of $\widetilde{A}_{0*}$, one should measure the energies of cell rearrangements. Hereafter, we explain the employed measurement method, focusing on parameter dependency only for the shape parameter $\widetilde{A}_0$ and the energy ratio *r*.

Measurement method

To investigate the energetic properties of cell rearrangement, we introduce a static model. In addition to the dynamical model mentioned previously, Equation (6) is adopted to describe the energy functional originating from the cell shape constraint, and one of the states corresponding to local energy minima is achieved from the random initial configuration of cell positions using the gradient descent method.

Using the final configuration that reaches the local energy minima, we measure the rearrangement energy for contacting pairs of cells. Figure 7 schematically expresses the difference of the adopted approach from that used in ref. [11]. For simplicity, we consider two-dimensional systems. In ref. [11], a cellular vertex model (CVM) was adopted, and variables represented the positions of vertices where three cells contacted each other; therefore, rearrangement was generated by shortening the edge length of the contacting cells to zero. Herein, on the contrary, we adopt the SPV model, where variables represent the positions of cell centers and the length of the edge cannot therefore be controlled. Instead of inducing length changes, cell centers are moved in

the opposite direction to each other, and cell pairs become disconnected after several iterations of this operation. In the case of the three-dimensional system, contacting edges are replaced with contacting faces, while both the process and its efficiency remain unchanged. The detailed procedures are explained in Supplementary Text S1.

Critical point and scaling behavior

The energy of a cellular rearrangement is denoted as ΔE. Figure 8 shows the distributions of ΔE rescaled with respect to its average over the sample faces ($\overline{\Delta E}$) for many parameter sets, revealing that good fits can be obtained using the k-gamma distribution ($p(x) = k^k x^{k-1} e^{(-kx)}/(k-1)!$, ($k = 1.38 \pm 0.01$)). This distribution reflects the maximization of entropy at a constant packing ratio and it is observed for many types of disordered systems [15,16].

Figure 9(a) shows $\overline{\Delta E}$ for different parameter sets. Depending on the magnitude of the energy ratio r, the finite values of $\overline{\Delta E}$ are different in regions where $\widetilde{A}_0$ is small. After rescaling via multiplication with r, three curves with similar forms are obtained (Fig. 9(b)). As measured here, the critical point $\widetilde{A}_{0*}$ exists within the range of 5.4–5.5. The rescaled rearrangement energy can possibly be used as a parameter to classify two phases. To examine the hypothesis that the phase transition occurs and the rescaled rearrangement energy vanishes at the critical point $\widetilde{A}_{0*}$, the measured data are scaled following a previously employed method [11]. In the Ising model for ferromagnetism, magnetization m is expressed as a function of magnetic field h and the $T - T_c$ temperature difference, where T_c is the critical temperature. In analogy with the relation in (m, h, $T - T_c$) for spin statistical physics, ($r\overline{\Delta E}$, r, $\widetilde{A}_0 - \widetilde{A}_{0*}$) should obey the scaling relation
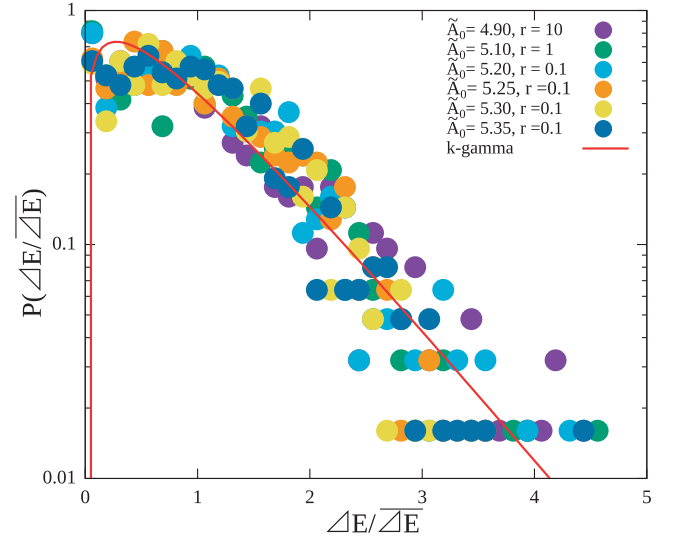

Figure 8 Distributions of re-scaled rearrangement energy for different parameter combinations, with 200 faces selected for each simulation. The red line shows the k-gamma distribution with $k = 1.38$.

$$r\overline{\Delta E} = |\widetilde{A}_0 - \widetilde{A}_{0*}|^\beta f_\pm \left(\frac{r}{|\widetilde{A}_0 - \widetilde{A}_{0*}|^\Delta} \right), \qquad (7)$$

where Δ is the crossover scaling critical exponent, and f_+ and f_- are the two branches of the crossover function whose sign added at its subscript corresponds to that of ($\widetilde{A}_0 - \widetilde{A}_{0*}$). Additionally, z is defined as $z = \frac{r}{|\widetilde{A}_0 - \widetilde{A}_{0*}|^\Delta}$ and represents the crossover scaling variable. The exponent β can be derived from the following relation in the limit $z \to 0$: $r\overline{\Delta E} \propto |\widetilde{A}_0 - \widetilde{A}_{0*}|^\beta$. At the critical point, the two branches
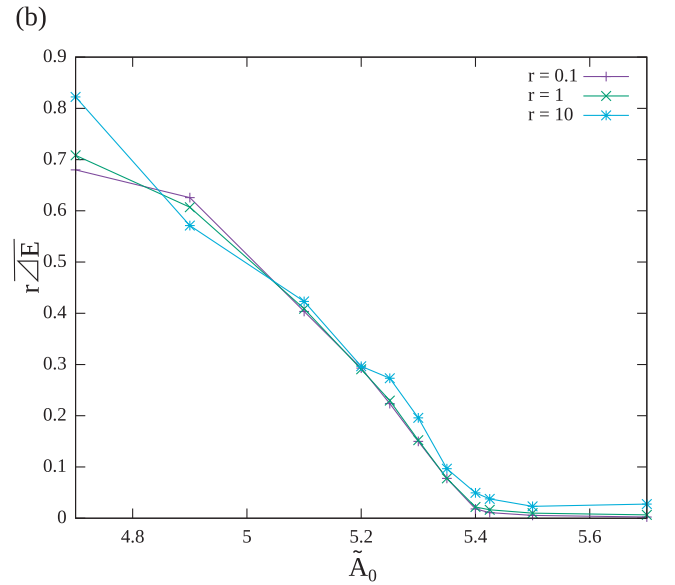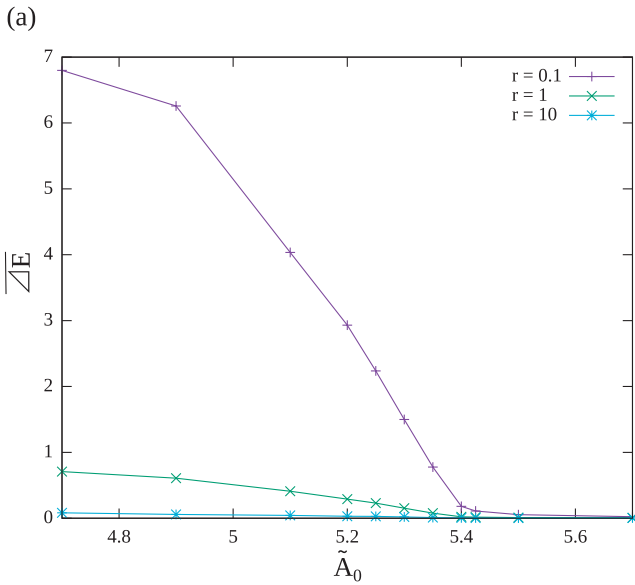

Figure 9 (a) Averaged energy of cell rearrangement ($\overline{\Delta E}$) and (b) rescaled averaged energy ($r\overline{\Delta E}$) as functions of $\widetilde{A}_0$ and r.
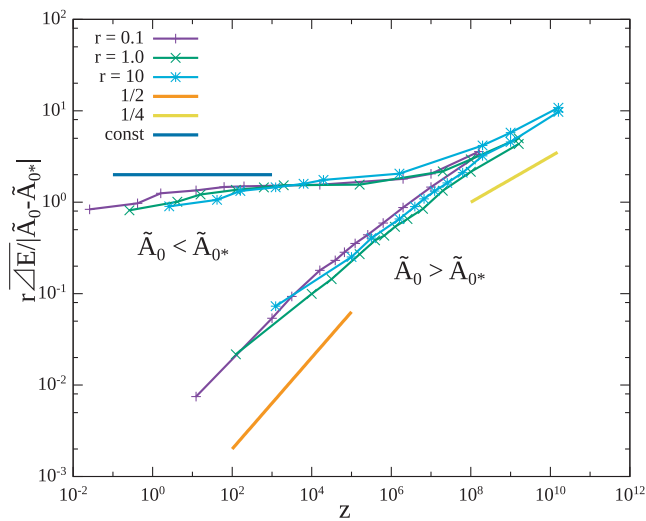
Figure 10   Scaling function determined for $(\widetilde{A}_{0*}, \beta, \Delta) = (5.410, 1, 4)$. Three slope lines are drawn to compare the universal curves with the fitted values of critical exponents.

merge as $f_+ = f_- = z^{\beta/\Delta}$. By changing the values of $\widetilde{A}_{0*}$ and using them to fit (β, Δ), we obtain the best fit for the scaling relation (Equation (7)) by taking $(\widetilde{A}_{0*}, \beta, \Delta) \sim (5.410, 1, 4)$ (Supplementary Text S2). With this set of values, the scaling function is obtained for z and collapses to a universal curve (Fig. 10). As seen in Section 3.1, the value of $\widetilde{A}_{0*}$ is not equal to that of the regular truncated octahedron. In the branch where cell rearrangement is highly suppressed by finite energy barriers, its height is scaled as $r\overline{\Delta E} \propto K_v V_0^2 (\widetilde{A}_0 - \widetilde{A}_{0*})$, while it is described as $r\overline{\Delta E} = r^{(\beta/\Delta)}$ in the limit $z \rightarrow \infty$.

The values of β and Δ are the same as those in the two-dimensional systems, as shown in [11]. This correspondence between systems of different dimensions is also observed for many types of systems that exhibit the jamming transition [2].

Conclusion and Discussion

In this study, we extend the techniques established in previous researches to probe the mechanical properties of three-dimensional tissues [11,12], showing that two types of collective motions, namely diffusive and sub-diffusive, emerge depending on the self-propulsion v_0 and the shape parameter $\widetilde{A}_0$. Sub-diffusive collective motions, occurring in the cases of caged cells and dynamic heterogeneity, are observed in the parameter region near the transition boundary line, in direct analogy to the behavior of glassy materials. Statistical analysis of individual cell shape reveals that the cell shape at the phase transition point does not correspond to a regular truncated octahedron but is more isotropic. To measure the critical value $\widetilde{A}_{0*}$ in the SPV model, we calculated rearrangement energy ΔE, whose average obeys the scaling relation (Equation (7)). The critical exponents were the same as those of two-dimensional tissues, indicating

that the upper critical dimension of the tissue equals two, i.e., equals that observed for glassy materials exhibiting the jamming transition.

At this point, we briefly discuss the possible relevance of our results to cell biology. First, EMT occurs in three-dimensional tissues, and its understanding is expected to shed light on various biological phenomena. Furthermore, some tissues such as skin and trachea can be regarded as pseudo-two-dimensional because they are only several-cell-thick in one direction. If the upper critical dimension of the tissue is two, the tissues are similarly considered to exhibit glassy properties because both two- and three-dimensional tissues also show these properties [11,12].

We did not consider the dynamics of single-cell mechanical properties such as elastic coefficients K_V and K_A and other types of interactions coupling v_0 and p_i. Consideration of this dynamics could lead to another type of collective motion, which may have a relation with chemotaxis and planar cell polarity. We assumed that tissues comprise cells with uniform mechanical properties; however, breaking this assumption may also trigger interesting phenomena.

In view of the fact that the shape index $\widetilde{A}_0$ can be experimentally measured, the results of this study were tested by assessing the mechanical properties of three-dimensional tissues. Furthermore, measurements of the shape index for all cells by three-dimensional imaging may unveil some anomalous events such as cancer metastasis.

Note

After the completion of this manuscript, we noted that a similar problem has been addressed in ref. [17], where it was determined that the critical point does not correspond to the global solution of tissue energy functionals. We, however, showed the scaling properties of cell rearrangement and phase transition energies, which are yet to be reported.

Acknowledgement

Conflicts of Interest

The author declares no conflicts of interest.

Author Contribution

The author directed the research and wrote the manuscript.

References

[1] Campbell, K. & Casanove, J. A common framework for EMT and collective cell migration. *Development* **143**, 4291–4300 (2016).

[2] Berthier, L. & Biroli, G. Theoretical perspective on the glass transition and amorphous materials. *Rev. Mod. Phys.* **83**, 587–645 (2011).

[3] Vicsek, T. Novel type of phase transition in a system of self-driven particles. *Phys. Rev. Lett.* **75**, 4 (1995).

[4] Marchetti, M. C., Joanny, J. F., Ramaswamy, S., Liverpool, T. B., Prost, J., Rao, M., *et al.* Hydrodynamics of soft active matter. *Rev. Mod. Phys.* **85**, 1143–1189 (2013).

[5] Ishihara, S. & Sugimura, K. Bayesian inference of force dynamics during morphogenesis. *J. Theor. Biol.* **313**, 201–211 (2012).

[6] Sugimura, K. & Ishihara, S. The mechanical anisotropy in a tissue promotes ordering in hexagonal cell packing. *Development* **140**, 4091–4101 (2013).

[7] Cochet-Escartin, O., Ranft, J., Silberzan, P. & Marcq, P. Border forces and friction control epithelial closure dynamics. *Biophys. J.* **106**, 65–73 (2014).

[8] Lee, M. H., Wu, P. H., Staunton, J. R., Ros, R., Longmore, G. D. & Wirtz, D. Mismatch in mechanical and adhesive properties induces pulsating cancer cell migration in epithelial monolayer. *Biophys. J.* **102**, 2731–2741 (2012).

[9] Palmieri, B., Bresler, Y., Wirtz, D. & Grant, M. Multiple scale model for cell migration in monolayers: Elastic mismatch between cells enhances motility. *Sci. Rep.* **5**, 11745 (2015).

[10] Schotz, E. M., Lanio, M., Talbot, J. A. & Manning, M. L. Glassy dynamics in three-dimensional embryonic tissues. *J. R. Soc. Interface* **10**, 20130726 (2013).

[11] Bi, D., Lopez, J. H., Schwarz, J. M. & Manning, M. L. A density-independent rigidity transition in biological tissues. *Nat. Phys.* **11**, 1074–1079 (2015).

[12] Bi, D., Yang, X., Marchetti, M. C. & Manning, M. L. Motility-driven glass and jamming transitions in biological tissues. *Phys. Rev. X* **6**, 021011 (2016).

[13] Schwarz, U. S. & Safran, S. A. Physics of adherent cells. *Rev. Mod. Phys.* **85**, 1327–1381 (2013).

[14] Weaire, D. & Phelan, R. A counter-example to Kelvin's conjecture on minimal surfaces. *Philos. Mag. Lett.* **69**, 107–110 (1994).

[15] Aste, T. & Di Matteo, T. Emergence of Gamma distributions in granular materials and packing models. *Phys. Rev. E* **77**, 021309 (2008).

[16] Newhall, K. A., Jorjadze, I., Vanden-Eijnden, E. & Brujic, J. A statistical mechanics framework captures the packing of monodisperse particles. *Soft Matter* **7**, 11518–11525 (2011).

[17] Merkel, M. & Manning, M. L. A geometrically controlled rigidity transition in a model for confluent 3D tissues. *New J. Phys.* **20**, 022002 (2018).